Food Research International 125 (2019) 108607

Contents lists available at ScienceDirect

Food Research International

journal homepage: www.elsevier.com/locate/foodres

Comparison of metabolic response between the planktonic and air-dried *Escherichia coli* to electrolysed water combined with ultrasound by ^{1}H NMR spectroscopy

Lin Zhao[a,c], Xue Zhao[a,c], Ji'en Wu[b], Xiaowei Lou[a,c], Hongshun Yang[a,c,*]

[a] Food Science and Technology Programme, c/o Department of Chemistry, National University of Singapore, 3 Science Drive 3, Singapore 117543, Singapore
[b] Setsco Services Pte Ltd, 18 Teban Gardens Crescent, Singapore 608925, Singapore
[c] National University of Singapore (Suzhou) Research Institute, 377 Lin Quan Street, Suzhou Industrial Park, Suzhou, Jiangsu 215123, PR China

ARTICLE INFO

Keywords:
Metabolomics
NMR
Principal component analysis
Oxidative stress
Pathway analysis
Air-dried cell
Stainless steel coupon
Omics

ABSTRACT

The antimicrobial effects of electrolysed water and ultrasound have been well reported; however, little attention was paid to their effects on the metabolite changes of bacteria in different states. In this study, the metabolomic variations of *Escherichia coli* ATCC 25922 in planktonic and adherent state (air-dried on stainless steel coupons) after the combination treatment of low-concentration acidic electrolysed water (AEW, free available chlorine (FAC): 4 mg/L) and ultrasound were characterised, by conducting multivariate data analysis based on nuclear magnetic resonance (NMR) spectroscopy. Overall, 43 metabolites were identified in two states of *E. coli*, including a wide range of amino acids, organic acids, nucleotides and their derivatives. The quantification of whole-cell metabolism in planktonic and air-dried cultures was quite different: air-dried *E. coli* exhibited more resistance to ultrasound and AEW treatments due to initiating a protective response against oxidative and acid stresses, which was not observed in planktonic *E. coli*, whose levels of all identified metabolites were decreased significantly after the combined treatment. Further pathway analysis revealed that alanine, aspartate and glutamate metabolism, glycolysis, pyruvate metabolism and tricarboxylic acid (TCA) cycle were changed significantly in planktonic culture, but to a less extent in air-dried culture, in which some shifts in glutamate decarboxylase (GAD) system and some shunts like mixed acid fermentation and pentose phosphate pathway were observed for maintaining metabolic balance. These findings suggest that NMR-based metabolomics strategy is promising in identifying different metabolic shifts in different states of bacteria. They also provide some guidance for food equipment sanitisation, especially for organic food processing.

1. Introduction

Organic food has faced increasing safety challenges accompanying by its rapid development over the past decades, due to using organic fertilisers and its highly perishable nature (Adhikari, Syamaladevi, Killinger, & Sablani, 2015; Chen, Zhang, Liu, Pang, Zhao, & Yang, 2019; Yu & Yang, 2017). Harvey, Zakhour, and Gould (2016) summarised 18 foodborne disease outbreaks caused by organic foods from 1992 to 2014, with 779 cases of illnesses, 258 hospitalisations and 3 deaths in the U.S., which could be attributed to a variety of pathogens, such as *Escherichia coli* O157:H7, *Salmonella* spp. and *Listeria monocytogenes*. In fact, organic food has great chance to be exposed to microbiological contamination at any point in food production, distribution and consumption. For example, during processing, work benches, conveyor belts and kitchen utensils can all play a role in transferring pathogens to food items (Heaton & Jones, 2008). Therefore, microbial control is an important part in organic food industry, especially for food contact surface sanitisation.

However, due to the strict regulations of organic operations, only limited numbers of chemical sanitisers are allowed to be used on the organic production line, including chlorine materials, hydrogen peroxide and ozone (USDA organic regulations 7 CFR 205.605, 2019). Electrolysed water (EW), which is produced by electrolysing dilute NaCl solution, has become increasingly popular in food industry as an effective sanitiser, due to its strong antimicrobial activity and safe characteristic (Liu, Jin, Feng, Yang, & Fu, 2019; Zhang & Yang, 2017; Zhao, Zhao, Phey, & Yang, 2019). However, the concentration of chlorine-based sanitisers allowed to use in organic food processing

* Corresponding author at: Food Science and Technology Programme, c/o Department of Chemistry, National University of Singapore, 3 Science Drive 3, Singapore 117543, Singapore.
E-mail address: chmynghs@nus.edu.sg (H. Yang).

https://doi.org/10.1016/j.foodres.2019.108607
Received 11 June 2019; Received in revised form 28 July 2019; Accepted 4 August 2019
Available online 06 August 2019
0963-9969/

cannot exceed 4 mg/L according to U.S. National Organic Program rules (NOP 5026, 2011). Therefore, low-concentration EW needs to be combined with another method to achieve a desirable sanitising effect, and ultrasound could be one choice, which can cause cavitational phenomenon to disrupt cellular structure and induce synergistic sanitising effect (Sagong et al., 2013).

Although the antimicrobial effects of EW and ultrasound have been well reported (Sánchez, Elizaquível, Aznar, & Selma, 2015; Zhao, Zhang, & Yang, 2017), little attention was paid to their effects on the bacterial metabolite changes, especially for low-concentration acidic electrolysed water (AEW, free available chlorine (FAC): 4 mg/L) meeting strict regulations of organic food. Metabolomics, as a novel "omics" approach in the post-genomic era, has become a powerful tool recently to profile metabolites of biological systems, discovering the differences between stressed and unstressed cells (Chen, Wu, Li, Liu, Zhao, & Yang, 2019; Zhao, Wu, Chen, & Yang, 2019).

Bacterial metabolomics is a comparatively late comer in the area of "omics" studies, however, with the improvement of analytical tools, screening larger number of intracellular metabolites becomes possible (Odeyemi, Burke, Bolch, & Stanley, 2018). For example, Jozefczuk et al. (2010) investigated *E. coli* from metabolite composition and gene expression levels respectively to describe its response to a variety of environmental perturbations, like the cold, heat and oxidative stress. Moreover, different states of bacteria are supposed to exhibit different metabolic responses even to same external treatments (Salaheen et al., 2016). For instance, the metabolic responses of *Pseudomonas fluorescens* to metal stress in planktonic and biofilm culture were quite distinct, as the latter could initiate a protective response (Booth et al., 2011). Therefore, as microbial colonisation on food contact surfaces (like plant processing equipment, household kitchen items) is a quite common phenomenon, its metabolomics study under sanitising treatment is of great significance in developing effective control strategy to ensure food safety.

Nuclear magnetic resonance (NMR) spectroscopy and mass spectrometry (MS) are two major equipment for metabolomics, both of which are able to identify global metabolites' structures and concentrations (Nicholson & Lindon, 2008). At present, NMR is the most used method in the research of microbial metabolomics, with uncomplicated sample preparation procedure. On the other hand, MS has higher sensitivity and reproducibility compared to NMR, making it possible to detect low concentration metabolites reliably, however, its quantitative ability might be compromised (Villas-Bôas, Mas, Åkesson, Smedsgaard, & Nielsen, 2005).

Considering global analysis of metabolite changes in different states of *E. coli* after low-concentration AEW and ultrasound combined treatment has not been performed, the main objective of this study was to evaluate the metabolomic variations of *E. coli* in planktonic state and adherent state (air-dried on stainless steel coupons) induced by the two stresses, by conducting multivariate data analysis based on NMR spectroscopy. This study would give a new insight into the antimicrobial mechanisms of low-concentration AEW and ultrasound based on metabolic profiling analysis.

2. Materials and methods

2.1. Bacterial strain and culture condition

E. coli ATCC 25922 was obtained from ATCC and in a 15% (*v*/v) glycerol stock at −80 °C. After transferred to tryptic soy broth (TSB, Oxoid, UK) and grown at 37 °C overnight for resuscitation, the bacterium was incubated on tryptic soy agar (TSA, Oxoid, UK) at 37 °C overnight to isolate a single colony, which was subcultured again in TSB for following use.

2.2. Treatment of planktonic cells

After grown to the stationary phase, *E. coli* cells (1 mL) was transferred to 200 mL freshly prepared TSB to grow at 37 °C overnight. A total of four bottles of 200 mL TSB containing *E. coli* were centrifuged at 8000 × *g* at 4 °C for 5 min (Eppendorf, Centrifuge 5804 R, Germany), followed by washing in phosphate-buffered saline (PBS, pH 7.2) twice, and the cell pellets were subject to four treatments respectively: (I) deionised water (DW, control group); (II) ultrasound (100 W, 22.5 kHz, JY92-IIN, Scientz, Ningbo, China); (III) AEW (with 4 mg/L FAC, generated by electrolysing 0.9% NaCl solution in an electrolysis device (ROX-10WB, Hoshizaki Singapore Pte Ltd)); (IV) the combination of AEW and ultrasound. For ultrasound alone (II) and combined (IV) treatments, the ultrasonic probe was immersed 2.0 cm into the DW and AEW solution, respectively. All treatment solutions were 5 mL and the treatment time was 5 min (for treatments containing ultrasound (II, IV), the total work time of ultrasonic processer was 5 min with every 5 s pulse and 5 s stop), after which the cell cultures were quenched on ice for 5 min and centrifuged (10,000 × *g*, 5 min, 4 °C) to remove the treatment solutions. The chilling method was used to stop the treatments by deactivating any unreacted molecules according to previous studies (Liu et al., 2017, 2018), as well as to avoid the addition of other chemical solvents to the extraction system. After washed with PBS for three times, cell pellets were resuspended in 3 mL of extraction solution (mixture of equal volumes of acetonitrile and $K_2HPO_4 - NaH_2PO_4$ buffer (0.1 M, pH 7.4)) for later metabolite extraction use.

2.3. Treatment of air-dried cells on the coupons

Stainless steel coupons (2.5 cm in side length and 1 mm in thickness, type: 304, Jinchengyu Metal Material Co., Shenzhen, China) were used as bacteria attached surface. After prepared according to the methods in our previous study (Zhao et al., 2017), the coupons were inoculated with 1 mL suspension of *E. coli* ATCC 25922 prepared in Section 2.1 and air-dried for 20 h in a laminar flow biosafety cabinet. The inoculated coupons were immersed in sterile 50 mL beakers containing 10 mL AEW (sterile 10 mL DW as control). For ultrasound alone and combined treatments, the beakers were placed in an ultrasonic tank (80 W, 37 kHz, Elmasonic S 30H, Siegen, Germany). After 5-min treatments, the adherent cells on coupons were scraped into solutions and centrifuged (10,000 × *g*, 5 min, 4 °C) to collect the pellets, which were washed by PBS twice and resuspended in 3 mL of extraction solution for following metabolite extraction use.

2.4. Extraction of intracellular metabolites

All cell pellets suspended in extraction solution (for both planktonic and air-dried cells) were sonicated on wet ice according to a previous method (Liu et al., 2017), with a total of 25 cycles and each cycle including 5 s pulses and 10 s stops. The supernatant containing metabolites from lysed cells was collected by centrifugation at 12,000 × *g* at 4 °C for 10 min, whereas the solid residues were homogenised again in the same volume of extraction solution using a vortex to get a secondary supernatant, which was pooled with the first one. The combined supernatants were condensed in vacuum to remove acetonitrile and water, and the rest of samples were stored at −80 °C for further NMR analysis.

2.5. NMR spectroscopic analysis

For NMR analysis, the samples were dissolved in deuterated water (D2O, 99.9%) containing 0.005% sodium 3-trimethylsilyl [2,2,3,3-d_4] propionate (TSP, Sigma-Aldrich, USA) and after centrifugation (12,000 × *g*, 10 min, 4 °C), 600 μL supernatants were pipetted into 5-mm NMR tubes. ^{1}H NMR measurements of *E. coli* extracts were performed at 25 °C on a Bruker DRX-500 NMR spectrometer (Bruker, Rheinstetten, Germany), which was equipped with a Triple Inverse Gradient probe operating at 500.23 MHz. The parameter settings for ^{1}H NMR spectra were based on a reported method (Liu et al., 2018; Ye et al., 2012), with recycle

delay (RD) 2 s, mixing time (t_m) 100 ms, t_1 6.5 μs and the 90° pulse length around 10 μs in a first increment of NOESY pulse sequence (recycle delay – 90° – t_1 – 90° – t_m – 90° – acquisition). Water suppression was conducted during RD and t_m by applying a weak continuous wave irradiation. 64 transients were obtained with a spectral width of 20 ppm and an acquisition time of 1.36 s into 32 k data points. Before Fourier transformation, all free induction decays were transformed by multiplying an exponential window function with a 1-Hz line broadening factor. The assays were done in triplicate.

2.6. Spectral processing and statistical analysis

The resulting NMR spectra were analysed using the software TopSpin 4.0.3 (Bruker, Rheinstetten, Germany), for the phase, baseline and TSP signal (0.0 ppm) corrections. After normalisation, the spectra were divided into the region buckets from 9.5 to 0.5 ppm with equal width of 0.004 ppm using the Amix package (version 3.9.15, Bruker). The water and acetonitrile regions were removed before the data sets were subject to multivariate analysis (SIMCA-P$^+$, version 11.0, Umetrics, Sweden). The principal component analysis (PCA) was performed to show the structure of each data set and the orthogonal projection to latent structure discriminant analysis (OPLS-DA) was conducted to analyse data in a scale of unit variance. Besides, the R^2X (representing the explained variables) and Q^2 (representing the model predictability) values were applied to evaluate the qualities of the models. The coefficient plots were related to the metabolite changes caused by ultrasound and AEW treatments and gained from back-transformed data. The colour-coded lines plotted by MATLAB R2018a (The Mathworks, Inc., Natick, USA) illustrated the weights of the discriminatory variables, with absolute values of correlation coefficients increasing from 0 to 1 while colour changing from blue to red (Lou et al., 2018). Lastly, the relevant metabolic pathways were investigated using MetaboAnalyst 4.0 (https://www.metaboanalyst.ca/) based on the metabolic response changes.

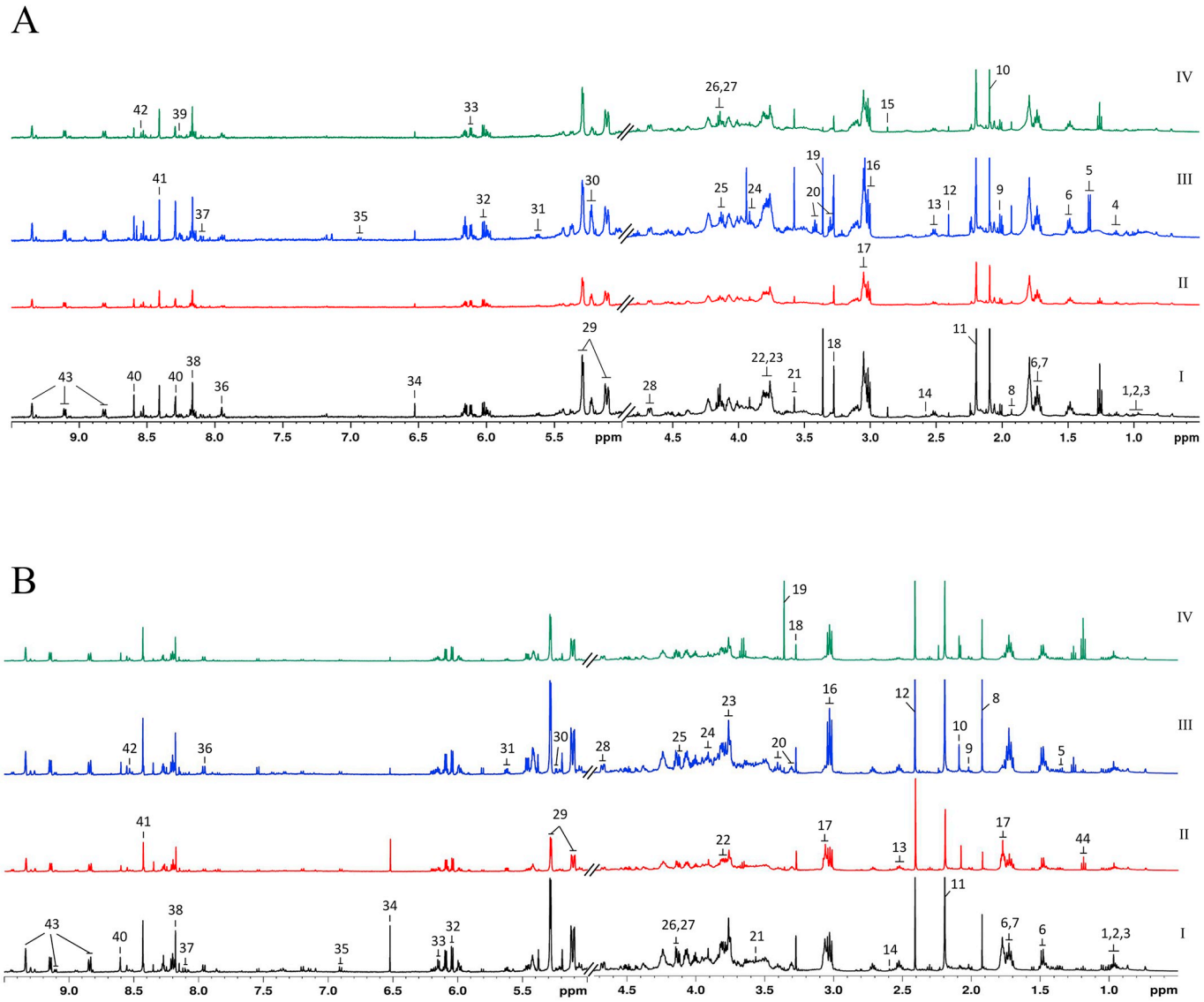

Fig. 1. Representative ^{1}H NMR spectra of planktonic *E. coli* extracts (A) and air-dried *E. coli* extracts (B) from different treatment groups. I: deionised water treatment; II: ultrasound treatment; III: acidic electrolysed water (AEW) treatment; IV: combination of AEW and ultrasound treatment. Metabolites: 1: isoleucine; 2: leucine; 3: valine; 4: β-hydroxybutyrate; 5: lactate; 6: lysine; 7: arginine; 8: acetate; 9: acetamide; 10: residual acetonitrile; 11: β-aminoadipate; 12: succinate; 13: aspartate; 14: methylamine; 15: trimethylamine; 16: γ-aminobutyrate; 17: putrescine; 18: betaine; 19: methanol; 20: taurine; 21: glycine; 22: alanine; 23: glutamate; 24: uridine; 25: glyceric acid; 26: phosphorylcholine; 27: *N*-acetyl alanine; 28: β-glucose; 29: phosphoenolpyruvate; 30: α-glucose; 31: ribose-5-phosphate; 32: cytidine; 33: adenosine 2′-3′-cyclic phosphate; 34: fumarate; 35: tyrosine; 36: xanthine; 37: uridine 5′-monophosphate (UMP); 38: hypoxanthine; 39: nicotinate; 40: adenosine monophosphate (AMP); 41: formate; 42: inosine triphosphate (ITP); 43: nicotinamide adenine dinucleotide (NAD); 44: ethanol.

Table 1
NMR data for metabolites of planktonic and air-dried *E. coli* extracts.

No.	Metabolites	δ^1 H (ppm) and multiplicity[a]
1	Isoleucine	0.96(t), 1.45(m)
2	Leucine	3.74(m), 1.73(m), 0.98(d), 0.96(d)
3	Valine	1.04(d), 0.99(d)
4	β-hydroxybutyrate	1.12(d)
5	Lactate	1.33(d), 4.11(q)
6	Lysine	1.48(d), 1.73(m), 3.03(t), 3.76(t)
7	Arginine	1.70(m), 3.76(t), 3.21(t)
8	Acetate	1.92(s)
9	Acetamide	2.01(s)
10	Residual acetonitrile	2.10(s)
11	β-aminoadipate	2.20(s)
12	Succinate	2.40(s)
13	Aspartate	2.52(dd)
14	Methylamine	2.58(s)
15	Trimethylamine	2.87(s)
16	γ-aminobutyrate	3.01(t)
17	Putrescine	3.04(t), 1.75(m)
18	Betaine	3.27(s), 3.91(s)
19	Methanol	3.36(s)
20	Taurine	3.30(t), 3.42(t)
21	Glycine	3.57(s)
22	Alanine	3.79(q), 1.48(d)
23	Glutamate	3.77(m), 1.95 (d), 2.08 (d)
24	Uridine	3.80(dd), 3.91(dd), 4.12(m), 4.22(dd), 4.34(dd)
25	Glyceric acid	4.13(m), 3.78(m)
26	Phosphorylcholine	4.14(d), 3.21(s)
27	*N*-acetyl alanine	4.14(q), 1.32(d), 2.03(s)
28	β-glucose	4.65(d), 3.30(t)
29	Phosphoenolpyruvate	5.30(d), 5.12(d)
30	α-glucose	5.23(d)
31	Ribose-5-phosphate	5.62(m), 4.11(m), 4.06(m), 4.22(m), 3.67(dd), 3.78(dd)
32	Cytidine	6.01 (d), 4.22(t)
33	Adenosine 2′-3′-cyclic phosphate	6.12(d), 7.97(s), 8.25(s), 5.43(m), 4.43(m), 3.91(m)
34	Fumarate	6.51(s)
35	Tyrosine	6.92 (d), 7.17(m), 3.91(dd), 3.06(dd)
36	Xanthine	7.95(s)
37	Uridine 5′-monophosphate (UMP)	8.10(d), 5.99(d)
38	Hypoxanthine	8.17(s), 8.20(s)
39	Nicotinate	8.26(s), 8.62(d), 8.49 (d), 7.53
40	Adenosine monophosphate (AMP)	8.28(s), 8.61(s), 6.12(d), 4.51(m), 4.37(m), 4.02(m)
41	Formate	8.41(s)
42	Inosine triphosphate (ITP)	8.54(s), 8.28(s), 6.15(d), 4.77(m), 4.40(m), 4.25(m)
43	Nicotinamide adenine dinucleotide (NAD)	9.34(s), 8.82(d), 8.18(m), 9.11(d), 6.11(d), 8.14(s), 8.41(s), 6.03(d)
44	Ethanol	1.19(t), 3.67

[a] Multiplicity: s, singlet; d, doublet; t, triplet; q, quartet; dd, doublet of doublets; m, multiplet.

For quantitative analysis, the concentration variation of metabolites was determined by comparing the integrals of each metabolite to that of TSP, which was served as an internal reference with known concentration (Bisht, Bhatnagar, Bisht, & Murthy, 2018). Mean values with standard deviation were compared using ANOVA ($P < .05$) and Duncan's multiple range test to assess the metabolite concentration differences among different treatment groups with an IBM SPSS statistical software (version 24; IBM Corp., Armonk, USA).

3. Results and discussion

3.1. ^{1}H NMR profile of planktonic and air-dried cells

The antimicrobial effects of ultrasound and AEW and their combination on planktonic *E. coli* cells were examined in our preliminary experiment, showing best effect in combined treatment group with around 4.5 log colony forming units (CFU)/mL reduction after 5 min, while ultrasound and AEW alone achieved only 1.0 and 3.8 log reduction, respectively (Fig. S1). However, beneath the reduction surface, these treatments also caused a series of metabolic changes in bacterial cells. The typical ^{1}H NMR spectra of metabolite extracts from both planktonic and air-dried *E. coli* cells after each treatment are shown in Fig. 1. The assignments of the peaks were determined by several NMR databases containing detailed information about biological compounds, such as the Biological Magnetic Resonance Data Bank (BMRB) and The *E. coli* Metabolome Database (ECMDB, http://www.ecmdb.ca/). According to the signals from 0.5 to 9.5 ppm, a total of 43 metabolites (exclude the acetonitrile residue) either from planktonic or air-dried cells were identified, including a range of essential primary and secondary metabolites, like the amino acids, organic acids, sugars, nucleotides and their derivatives.

The typical ^{1}H NMR spectra of *E. coli* extracts from both planktonic and air-dried cells on coupons displayed high similarity in metabolite variety, with a majority of amino acids both concentrated in the region of 0.5–4.0 ppm, such as lysine, aspartate, taurine, alanine and glutamate (Fig. 1A, B). Besides, in the range between 5.0 and 9.0 ppm, aromatic compounds like adenosine 2′-3′-cyclic phosphate and nucleotides like cytidine, AMP and UMP were shown in both states of *E. coli*. Furthermore, the intensity and the diversity of some metabolite signals were different among the four treatment groups in each state of *E. coli*. For instance, the ^{1}H signal at 1.33 ppm, which was assigned as lactate, was detected in the spectra of planktonic *E. coli* after AEW treatment, whereas not detectable in other three counterparts (Fig. 1A). Decreased solubility of oxygen in AEW could be one possible reason for lactate production, through mixed acid fermentation (Ebrahimi, Larsen, Jensen, Vogensen, & Engelsen, 2016). A similar result also happened in the air-dried *E. coli* extracts, with ethanol signal (1.19 ppm) only detectable in groups containing ultrasound treatment (Fig. 1B), as ultrasound could promote ethanol production by enhancing the secretion of related enzyme (Velmurugan & Incharoensakdi, 2016). The resonance assignments of key identified metabolites either from planktonic or air-dried cells are summarised in Table 1.

3.2. Principal components analysis

To investigate the effects of ultrasound and low-concentration AEW on the metabolite profiles of different states of *E. coli*, PCA analysis was carried out, providing an overview of the metabolic changes during 5-min stresses by screening the principle metabolites.

For planktonic *E. coli* analysis, the first two principal components (PC1 and PC2) explained 93.1% of the total variance obtained from the four treated groups, with PC1 explaining 66.1% (Fig. 2A1). The visual inspection of score plot demonstrated that the samples from the four treatment groups were separated clearly into four clusters, each of which contained the samples from the same treatment group (Fig. 2A2). The control (I) and the AEW group (III) were both located in the positive side of PC1, however, they tended to be in the opposite sides of PC2 compared with those of group II (ultrasound alone) and IV (ultrasound combined with AEW), the two of which were negatively and mainly influenced by PC1.

PCA analysis of *E. coli* extracts from air-dried cells on coupons were significantly different compared to that of planktonic cells, with lower R^2X and Q^2 values of both PC1 and PC2, indicating the model fitness might be compromised relatively (Fig. 2B1). Moreover, group I and II were negatively affected by PC1 and located in the opposite sides of PC2, while group III and IV were clustered in the positive side of PC1 and influenced differently by PC2 (Fig. 2B2).

PCA is a powerful tool to investigate the discriminative factors from collected NMR spectra (Gjersing, Herberg, Horn, Schaldach, & Maxwell, 2007). In this study, the high R^2X values (0.931 and 0.919 for planktonic and air-dried cells respectively) and Q^2 values (0.892 and 0.839 for planktonic and air-dried cells respectively) of the first two principal components showed the good fitness of the model for both states of *E.*

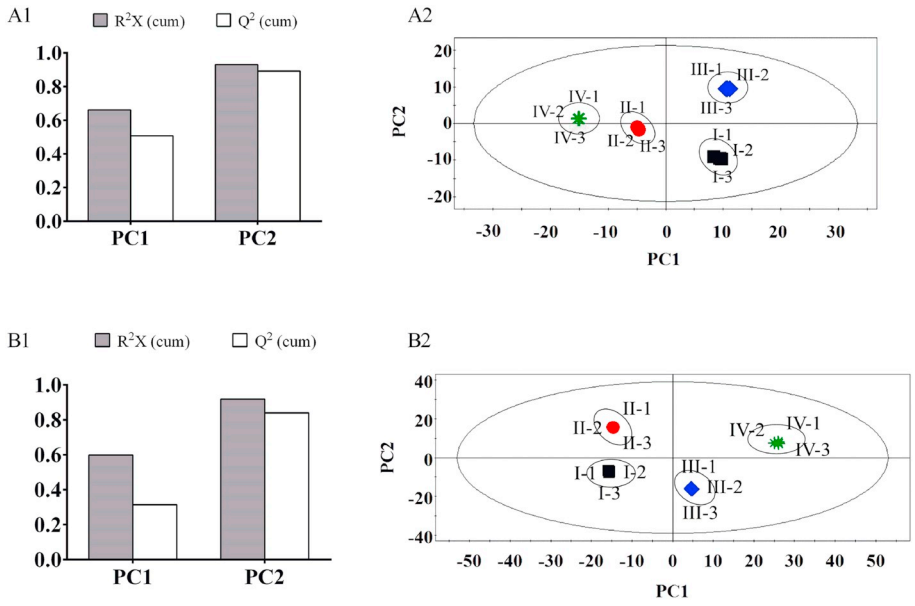

Fig. 2. Principal component analysis (PCA) for the metabolite profile of planktonic *E. coli* extracts (A1 and A2) and air-dried *E. coli* extracts (B1 and B2). A1 and B1: the principal components explaining variances used in PCA; A2 and B2: the score plot of PCA. Note: R^2X: explained variable value; Q^2: model predictability value; I: deionised water treatment; II: ultrasound treatment; III: acidic electrolysed water (AEW) treatment; IV: combination of AEW and ultrasound treatment.

coli. The distinct clusters revealed dramatic metabolic differences among these four treatment groups, however, to further study the associated metabolites responsible for the class separation, pairwise comparative tool OPLS-DA should be used to show intergroup metabolomic differences (Wiklund et al., 2008).

3.3. Alterative metabolites during ultrasound and AEW stresses

Based on the PCA results, OPLS-DA was constructed in the following pairwise groups: I and II; I and III; I and IV; II and IV; III and IV. I, II, III and IV was deionised water, ultrasound, AEW and ultrasound + AEW treatment, respectively. The five pairwise groups were compared for both planktonic and air-dried *E. coli* cells, respectively, as shown in Figs. 3 and 4.

Among the five pairwise comparisons for the metabolite changes of planktonic *E. coli* extracts, the groups containing ultrasound treatment (II and IV) showed downward peaks of all identified metabolites when compared to the control group (I), indicating ultrasound induced a significant decrease of a wide range of metabolite contents in planktonic *E. coli* (Fig. 3A, C). On the other hand, in comparison to control group, AEW treatment alone (III) elicited a significant increase in the levels of leucine, valine, taurine, glycine, arginine, lactate, succinate, acetate and acetamide, however, when combined with ultrasound, opposite trend happened (Fig. 3B, C). In fact, the lowest level of most metabolites belonged to the combined treatment group (IV), with further decreasing trends compared to each treatment used alone (Fig. 3D, E). Moreover, all pairwise comparisons showed strong separation and high predictability (with all $R^2X > 0.639$, $Q^2 > 0.933$, data not shown) of the OPLS-DA model (Fig. 3A–E left sides), indicating significant intergroup differences and good model fitness.

Fig. 4 shows the biochemical levels of air-dried *E. coli* extracts, which were significantly different to the planktonic counterpart. According to the coefficient-loading plots (Fig. 4 right sides), AEW induced elevated levels of a wide range of metabolites, such as acetate, β-aminoadipate, taurine, alanine, glutamate, glucose and xanthine, whereas reduced the contents of putrescine, uridine, cytidine, fumarate and AMP, compared to the control group (Fig. 4B). Although the ultrasound alone caused decreased levels of most identified metabolites, like a variety of amino acids and organic acids concentrated in the region of 0.5–4.0 ppm (Fig. 4A), when combined with AEW, upward trends were presented, showing the most abundant contents of most metabolites among four groups (Fig. 4CDE). Similar to the high cross-validation parameters of OPLS-DA model for the planktonic *E. coli* extracts, the R^2X and Q^2 values for all pairwise comparisons of air-dried *E. coli* were also > 0.701 and 0.978, respectively, indicating clear group separation and equal model's suitability for analysing attached cells' metabolites (Fig. 4A–E left sides, data not shown).

It has been believed that HOCl and $^{-}$OCl, the major chlorine compounds in AEW, could inhibit microbial growth by changing a series of biological functions, such as membrane transport capacity and enzyme activity (Hussain, Tango, & Oh, 2019; Sow, Tirtawinata, Yang, Shao, & Wang, 2017). Moreover, AEW could induce reactive oxygen species (ROS) production in bacteria, such as superoxide anion ($\dot{O}_2^-$), hydrogen peroxide (H_2O_2) and hydroxyl radical ($\dot{O}H$), which can interact with biomolecules and cause their oxidative modifications to accelerate necrosis and apoptosis of bacteria (Wall, Oh, Diers, & Landar, 2012). Therefore, a wide range of metabolic changes such as DNA modification, phospholipid damage and irreversible protein oxidation observed in this study were in agreement with previous reports, due to various reactive groups these biomolecules contain, like the thiol groups, amino groups and peptide bonds, which were sensitive to oxidative stress and induced a series of metabolic reactions (Nightingale et al., 2000).

On the other hand, ultrasound has been reported to elicit both mechanical effects (shock waves, microstreaming, etc.) and sonochemical reactions (free radicals) to disrupt bacteria (Bastarrachea, Walsh, Wrenn, & Tikekar, 2017). Although there is still no consensus about ultrasound's antimicrobial mechanisms, acoustic cavitation is most universally accepted, causing multifactorial changes of microbial cells. Li et al. (2018) found the levels of extracellular H_2O_2 and intracellular ROS in *E. coli* O157:H7 were increased significantly by ultrasonic processing, while the adenosine triphosphate (ATP) level of the cells was reduced, which could be served as possible apoptosis-inducing factors caused by ultrasonic actions. Considering cell membrane permeability was not changed significantly after ultrasound treatment in our previous study (Zhao et al., 2017), the decreased levels of a wide range of metabolitles shown in Fig. 3A indicated that the alterations in metabolic performance induced by these apoptosis-related factors could be happened during ultrasound stress.

More importantly, the combination of AEW and ultrasound exhibited some synergistic effects, which might be attributed to several mechanisms. First, ultrasound could scatter the bacterial clusters into single cells, increasing their interaction opportunities with AEW. Besides, the cavitation bubbles generated by ultrasound could damage cell membranes, increasing penetration rate of AEW into the cells.

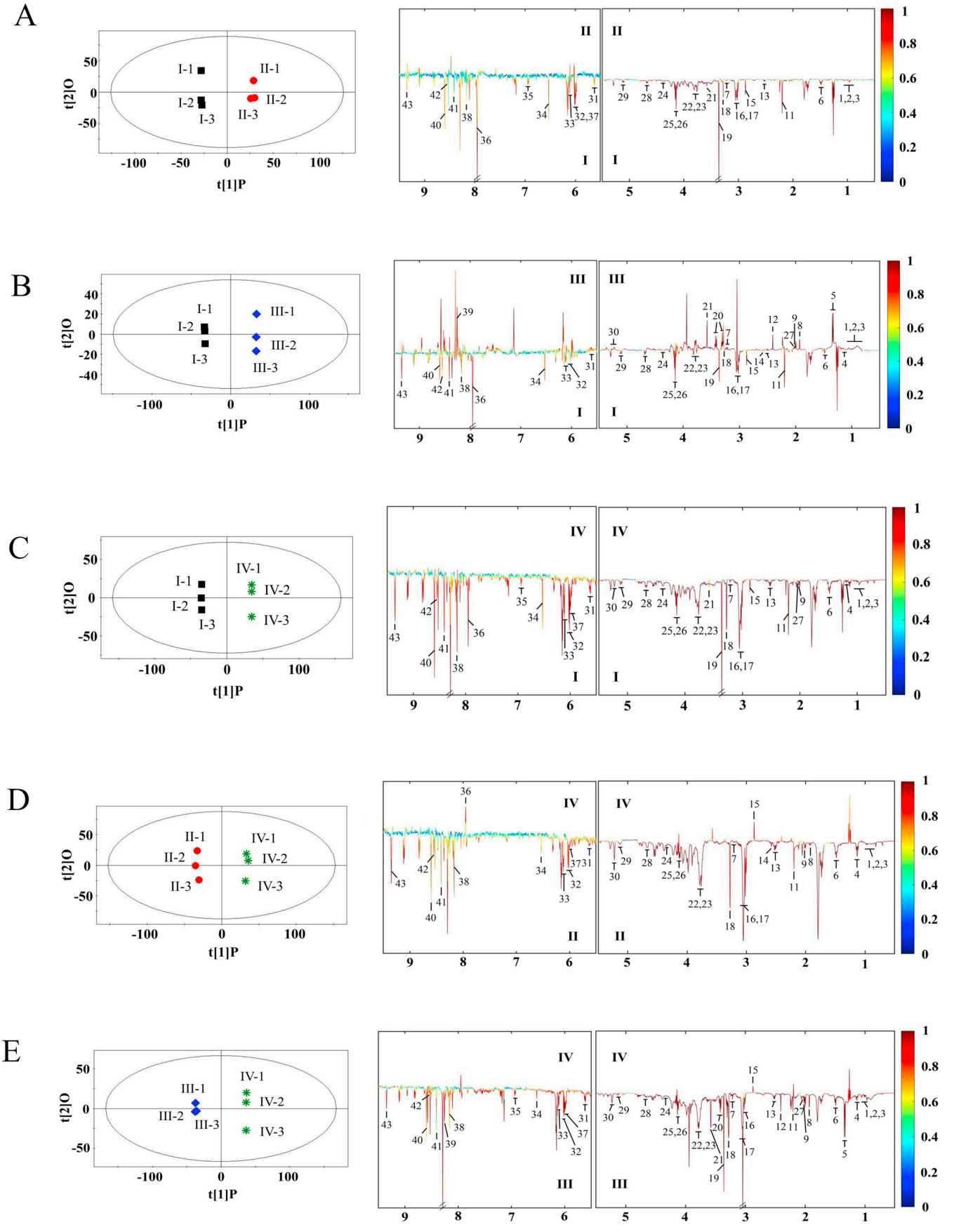

(caption on next page)

Fig. 3. Orthogonal projection to latent structure discriminant analysis (OPLS-DA) score plots (left) and coefficient-coded loading plots (right) for planktonic *E. coli* extracts. (A) Comparison results between group I (black square) and group II (red circle); (B) Comparison results between group I (black square) and group III (blue diamond); (C) Comparison results between group I (black square) and group IV (green star); (D) Comparison results between group II (red circle) and group IV (green star); (E) Comparison results between group III (blue diamond) and group IV (green star). I: deionised water treatment; II: ultrasound treatment; III: acidic electrolysed water (AEW) treatment; IV: combination of AEW and ultrasound treatment. Metabolites keys to the numbers are the same as Fig. 1. (For interpretation of the references to colour in this figure legend, the reader is referred to the web version of this article.)

Moreover, the damaged cells could be further broken up by ultrasound, causing membrane integrity loss and cell death (Li et al., 2017).

It was also interesting to notice the different metabolic changes of planktonic and air-dried *E. coli* under ultrasound and AEW stresses. Once bacteria attach to the surface, more resistance will be shown to antimicrobial treatments than their planktonic counterparts, and the synergistic mechanisms of ultrasound and AEW combination mentioned above might not be applied on attached cells (Maifreni et al., 2015). In this study, the air-dried *E. coli* cells located at or near the surface of the dried inoculum could serve as protection barriers for cells of internal layers, improving their antimicrobial resistance and resulting in their corresponding metabolic differences compared to the planktonic response. Moreover, the dried cells on stainless steel coupons might undergo starvation during 20 h drying accompanied by a series of metabolic changes, which could also increase bacteria resistance to help them survive under this combined treatment, a possible cause associated with increased metabolite levels observed in Fig. 4 (Kim, Ryu, & Beuchat, 2007).

3.4. Metabolite quantification analysis

In order to get more detailed information about the metabolite changes under different stresses, the concentrations of identified metabolites without overlapping chemical shifts were quantified and shown in Table 2 (for planktonic *E. coli*) and Table 3 (for air-dried *E. coli*), respectively.

Correlation coefficient values were used to evaluate each variable's contribution to a total class discrimination. In this study, the absolute coefficient value of 0.602 was applied as a cutoff point to determine the statistical significance (Ye et al., 2013). The coefficient test revealed that among all of the identified metabolites, around 30 (including a wide range of amino acids, organic acids and nucleotides) played an important role in discriminating stressed *E. coli* cells from the normal cells, with obvious concentration variation among four treatment groups in the two bacteria states (Tables 2 and 3).

Energy associated metabolism is a prime target for “attack” under stresses. In planktonic culture of our study, a significant drop of glucose level was observed during ultrasound and AEW combined treatment, indicating energy was needed in response to the stress. Whereas in the air-dried cells, the glucose level was not changed so significantly after the combined treatment, showing an energy conservation strategy adopted by the dried cells, to maintain lasting energy for their survival (Jozefczuk et al., 2010). Meanwhile, phosphoenolpyruvate, an important intermediate involved in glycolysis and gluconeogenesis, was detected in this study. Considering phosphoenolpyruvate could be converted to pyruvate in the generation of ATP, its lower level in planktonic and air-dried *E. coli* after ultrasound and AEW combined treatment also indicated a perturbation of energy metabolism, albeit in different degrees (Ye et al., 2012).

Amino acids are also major targets during oxidative and osmotic stresses. As mentioned in Section 3.3, ultrasound and AEW could both stimulate ROS generation in bacterial cells, inducing amino acid oxidase system and decreasing amino acid levels (Lushchak, 2011). In this study, a marked depletion of isoleucine, leucine, valine, lysine, arginine and alanine levels in planktonic *E. coli* cells were observed after combined treatment, due to their sensitivity to oxidation (Feng, Yang, & Hielscher, 2008). On the other hand, amino acids can play a role in maintaining the stabilisation of cell osmolarity, which can explain why some amino acid levels (isoleucine, leucine, valine, lysine, etc.) in air-dried cells were increased under ultrasound and AEW stresses, showing the effort for survival and the attached cell's resistance in response to stresses (Malmendal et al., 2006). In addition, as a most common and effective osmoprotectant in *E. coli*, betaine can relieve osmotic stress by controlling protein disaggregation and synthesis (Miranda, Campos-Galvão, & Nero, 2018). As shown in Table 2, the content of betaine in planktonic *E. coli* cells was decreased significantly after ultrasound treatment, and when combined with AEW, the situation was even worse. However, its level in air-dried *E. coli* cells was relatively stable after all treatments, thus could protect the cells from osmotic stress (Table 3).

The biosynthesis of nucleotides was also influenced under the stresses, such as cytidine and uridine, whose levels in the planktonic *E. coli* cells were decreased more after ultrasound and AEW combined treatment than each used alone. However, in the air-dried *E. coli* cells, these two contents were increased after combined treatment, showing opposite trends compared to other groups and reflecting air-dried cell's resistance. Concomitantly, ribose-5-phosphate, as the precursor for nucleotide synthesis, exhibited a decreasing level in the planktonic *E. coli* cells after all treatments, making depressed nucleotide biosynthesis reasonable (Jozefczuk et al., 2010).

3.5. Pathway analysis

To investigate the metabolic responses to ultrasound and AEW stresses globally, analysis of related metabolic pathways in different states of *E. coli* is necessary, providing a more in-depth understanding of metabolic network activity on a comprehensive basis. By using MetaboAnalyst 4.0, a total of 44 pathways were predicted and listed in Table S1, according to the metabolite involvement in each state of *E. coli*.

The pathways with a false discovery rate $P < .05$ were considered as the most relevant metabolic pathways affected by stress exposure (Liu et al., 2018). For the planktonic *E. coli* cells, 12 biological pathways were suggested to be most likely to be affected by the ultrasound and AEW stresses, including aminoacyl-tRNA biosynthesis; alanine, aspartate and glutamate metabolism; nitrogen metabolism; butanoate metabolism; arginine and proline metabolism; methane metabolism; nicotinate and nicotinamide metabolism; pyruvate metabolism; glycolysis or gluconeogenesis; glycine, serine and threonine metabolism; cyanoamino acid metabolism and citrate cycle (TCA cycle). A similar finding was shown in air-dried *E. coli* cells, with also 12 key pathways in response to ultrasound and AEW stresses but nicotinate and nicotinamide metabolism substituted by glutathione metabolism (Table S1). In addition, an overview of all matched pathways was displayed in Fig. 5 as circles, expressing the *P* value and the impact value of each pathway through the colour and size, respectively.

These results show again that the metabolic responses to ultrasound and AEW stresses were very different between planktonic and air-dried *E. coli* cells, based on an overall profile of metabolic network. The main pathways affected by the combined treatment in *E. coli* of each state are summarised and shown in Fig. 6, including carbohydrate metabolism, amino acid metabolism, nucleotide metabolism and fatty acid metabolism.

Glycolysis is the most fundamental pathway of glucose consumption and its end-product, pyruvate, is changed into acetyl-CoA by decarboxylation and goes into the tricarboxylic acid (TCA) cycle under

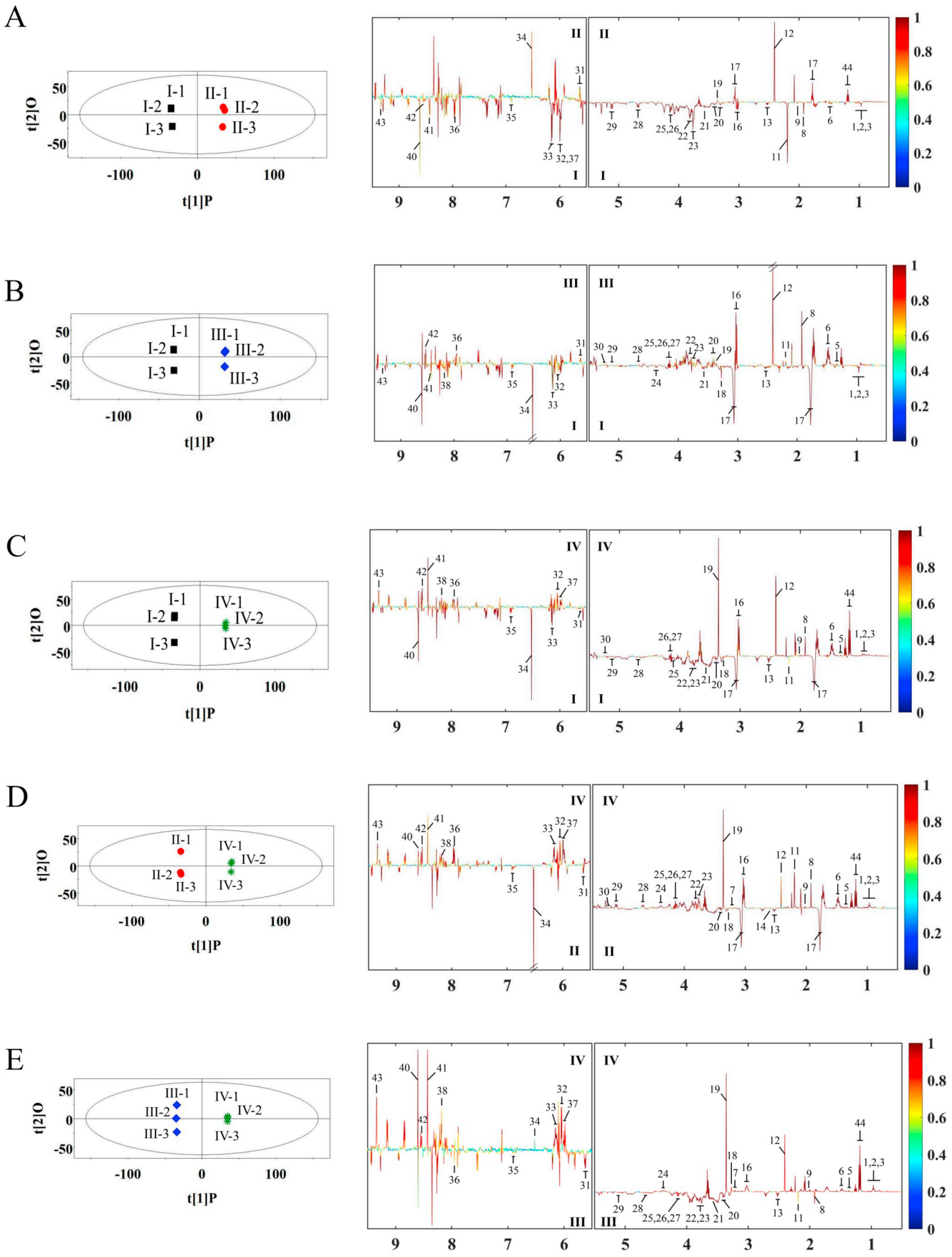

(caption on next page)

Fig. 4. Orthogonal projection to latent structure discriminant analysis (OPLS-DA) score plots (left) and coefficient-coded loading plots (right) for air-dried *E. coli* extracts. (A) Comparison results between group I (black square) and group II (red circle); (B) Comparison results between group I (black square) and group III (blue diamond); (C) Comparison results between group I (black square) and group IV (green star); (D) Comparison results between group II (red circle) and group IV (green star); (E) Comparison results between group III (blue diamond) and group IV (green star). I: deionised water treatment; II: ultrasound treatment; III: acidic electrolysed water (AEW) treatment; IV: combination of AEW and ultrasound treatment. Metabolites keys to the numbers are the same as Fig. 1. (For interpretation of the references to colour in this figure legend, the reader is referred to the web version of this article.)

Table 2
Coefficients from OPLS-DA and metabolite contents in planktonic *E. coli* after different treatments.

Metabolites	Coefficient[1]					Contents (mg/L)[2]			
	II/I	III/I	IV/I	IV/II	IV/III	I	II	III	IV
Isoleucine	−0.96	0.97	−0.98	−0.95	−0.99	0.52 ± 0.01^{a}	0.38 ± 0.00^{b}	0.54 ± 0.02^{a}	0.27 ± 0.01^{c}
Leucine	−0.98	0.98	−0.99	−0.97	−0.99	0.33 ± 0.01^{b}	0.22 ± 0.00^{c}	0.36 ± 0.01^{a}	0.15 ± 0.00^{d}
Valine	−0.97	0.98	−0.92	−0.94	−0.99	0.46 ± 0.01^{b}	0.34 ± 0.00^{c}	0.51 ± 0.02^{a}	0.27 ± 0.00^{d}
β-hydroxybutyrate	−0.21	−0.87	−0.95	−0.99	−0.99	0.18 ± 0.01^{a}	0.15 ± 0.00^{b}	0.18 ± 0.00^{a}	0.08 ± 0.00^{c}
Lactate	−0.81	0.99	−0.93	−0.97	−0.99	0.36 ± 0.00^{b}	0.30 ± 0.00^{c}	1.16 ± 0.03^{a}	0.22 ± 0.00^{d}
Lysine	−0.97	−0.97	−0.99	−0.98	−0.99	3.27 ± 0.01^{a}	2.31 ± 0.01^{c}	2.62 ± 0.12^{b}	1.53 ± 0.01^{d}
Arginine	−0.96	0.99	−0.96	−0.93	−0.99	0.81 ± 0.01^{b}	0.63 ± 0.02^{c}	0.97 ± 0.06^{a}	0.45 ± 0.01^{d}
Acetate	−0.77	0.99	−0.99	−0.83	−0.99	0.16 ± 0.00^{b}	0.14 ± 0.00^{c}	0.24 ± 0.01^{a}	0.10 ± 0.00^{d}
Acetamide	−0.55	0.99	−0.95	−0.94	−0.99	0.19 ± 0.00^{b}	0.15 ± 0.00^{c}	0.20 ± 0.01^{a}	0.11 ± 0.00^{d}
β-aminoadipate	−0.99	−0.99	−0.99	−0.85	−0.97	4.51 ± 0.06^{a}	3.04 ± 0.03^{b}	3.15 ± 0.16^{b}	2.45 ± 0.02^{c}
Succinate	−0.64	0.99	−0.41	−0.63	−0.98	0.10 ± 0.00^{b}	0.07 ± 0.00^{c}	0.21 ± 0.01^{a}	0.07 ± 0.00^{c}
Aspartate	−0.96	−0.82	−0.99	−0.98	−0.99	3.60 ± 0.05^{a}	2.68 ± 0.02^{c}	3.24 ± 0.19^{b}	1.58 ± 0.02^{d}
Methylamine	−0.36	−0.74	−0.97	−0.97	−0.96	0.03 ± 0.00^{a}	0.03 ± 0.00^{b}	0.03 ± 0.00^{c}	0.02 ± 0.00^{d}
Trimethylamine	−0.99	−0.99	−0.99	0.98	0.91	0.04 ± 0.00^{a}	0.00 ± 0.00^{c}	0.00 ± 0.00^{c}	0.01 ± 0.00^{b}
γ-aminobutyrate	−0.98	−0.99	−0.98	−0.99	−0.95	5.29 ± 0.01^{a}	3.41 ± 0.03^{b}	3.25 ± 0.17^{b}	2.26 ± 0.02^{c}
Putrescine	−0.99	−0.99	−0.99	−0.99	−0.99	4.50 ± 0.04^{a}	3.11 ± 0.02^{c}	3.58 ± 0.2^{b}	1.87 ± 0.01^{d}
Betaine	−0.97	−0.50	−0.98	−0.84	−0.99	0.35 ± 0.00^{a}	0.21 ± 0.00^{c}	0.30 ± 0.02^{b}	0.08 ± 0.00^{d}
Methanol	−0.99	−0.92	−0.99	−0.57	−0.98	0.43 ± 0.00^{a}	0.02 ± 0.00^{c}	0.25 ± 0.02^{b}	0.02 ± 0.00^{c}
Taurine	−0.98	0.99	−0.99	−0.97	−0.99	1.13 ± 0.01^{b}	0.78 ± 0.01^{c}	1.76 ± 0.10^{a}	0.58 ± 0.01^{d}
Glycine	−0.95	0.99	−0.65	−0.69	−0.99	0.63 ± 0.00^{b}	0.40 ± 0.00^{c}	1.02 ± 0.06^{a}	0.37 ± 0.00^{c}
Alanine	−0.98	−0.99	−0.99	−0.98	−0.99	11.94 ± 0.10^{a}	8.30 ± 0.08^{c}	10.58 ± 0.53^{b}	5.50 ± 0.04^{d}
Glutamate	−0.98	−0.99	−0.99	−0.99	−0.99	18.84 ± 0.11^{a}	13.27 ± 0.11^{c}	17.13 ± 0.83^{b}	8.65 ± 0.09^{d}
Uridine	−0.99	−0.70	−0.99	−0.99	−0.99	3.05 ± 0.02^{a}	2.21 ± 0.02^{c}	2.65 ± 0.14^{b}	1.49 ± 0.02^{d}
Glyceric acid	−0.98	−0.91	−0.99	−0.98	−0.99	3.97 ± 0.02^{a}	2.65 ± 0.03^{c}	3.44 ± 0.17^{b}	1.81 ± 0.02^{d}
Phosphorylcholine	−0.99	−0.99	−0.99	−0.84	−0.98	5.76 ± 0.01^{a}	2.92 ± 0.02^{c}	3.41 ± 0.16^{b}	2.28 ± 0.01^{d}
N-acetyl alanine	−0.93	0.99	−0.97	−0.93	−0.99	0.37 ± 0.00^{b}	0.28 ± 0.00^{c}	0.39 ± 0.02^{a}	0.22 ± 0.00^{d}
β-glucose	−0.97	−0.97	−0.97	−0.96	−0.98	3.54 ± 0.04^{a}	2.38 ± 0.02^{c}	2.65 ± 0.11^{b}	1.68 ± 0.05^{d}
Phosphoenolpyruvate	−0.98	−0.99	−0.96	−0.88	−0.91	2.68 ± 0.09^{a}	1.88 ± 0.07^{b}	1.94 ± 0.13^{b}	1.48 ± 0.05^{c}
α-glucose	−0.90	0.99	−0.99	−0.97	−0.99	1.17 ± 0.04^{b}	1.04 ± 0.03^{c}	1.29 ± 0.07^{a}	0.44 ± 0.02^{d}
Ribose-5-phosphate	−0.83	−0.82	−0.96	−0.84	−0.95	0.70 ± 0.03^{a}	0.51 ± 0.02^{b}	0.66 ± 0.04^{a}	0.34 ± 0.03^{c}
Cytidine	−0.95	−0.36	−0.94	−0.87	−0.89	1.24 ± 0.01^{a}	0.95 ± 0.03^{b}	1.02 ± 0.06^{b}	0.64 ± 0.02^{c}
Adenosine 2′-3′-cyclic phosphate	−0.84	−0.75	−0.92	−0.90	−0.90	1.63 ± 0.02^{a}	1.27 ± 0.03^{b}	1.30 ± 0.09^{b}	0.84 ± 0.04^{c}
Fumarate	−0.80	−0.91	−0.76	−0.61	−0.83	0.07 ± 0.00^{a}	0.04 ± 0.00^{b}	0.04 ± 0.00^{b}	0.02 ± 0.00^{c}
Tyrosine	−0.90	−0.34	−0.91	−0.45	−0.86	0.09 ± 0.01^{a}	0.05 ± 0.01^{b}	0.08 ± 0.01^{a}	0.03 ± 0.01^{b}
Xanthine	−0.99	−0.99	−0.99	0.98	−0.11	0.45 ± 0.01^{a}	0.13 ± 0.02^{b}	0.16 ± 0.02^{b}	0.16 ± 0.00^{b}
UMP	−0.98	−0.97	−0.98	−0.86	−0.98	0.76 ± 0.00^{a}	0.50 ± 0.02^{c}	0.70 ± 0.04^{b}	0.36 ± 0.02^{d}
Hypoxanthine	−0.58	−0.88	−0.96	−0.96	−0.69	0.71 ± 0.00^{a}	0.56 ± 0.01^{b}	0.55 ± 0.03^{b}	0.37 ± 0.01^{c}
Nicotinate	−0.34	0.99	−0.44	−0.50	−0.99	0.08 ± 0.00^{b}	0.06 ± 0.01^{c}	0.16 ± 0.01^{a}	0.04 ± 0.01^{d}
AMP	−0.72	−0.96	−0.99	−0.82	−0.78	0.97 ± 0.03^{a}	0.60 ± 0.02^{c}	0.69 ± 0.04^{b}	0.29 ± 0.02^{d}
Formate	−0.50	−0.92	−0.93	−0.60	−0.56	0.21 ± 0.00^{a}	0.16 ± 0.00^{b}	0.17 ± 0.01^{b}	0.11 ± 0.00^{c}
ITP	−0.58	−0.68	−0.92	−0.97	−0.83	0.69 ± 0.04^{a}	0.52 ± 0.03^{b}	0.46 ± 0.03^{b}	0.35 ± 0.03^{c}
NAD	−0.82	−0.86	−0.98	−0.98	−0.95	2.71 ± 0.02^{a}	2.19 ± 0.04^{b}	2.05 ± 0.12^{b}	1.46 ± 0.02^{c}

Note: UMP: uridine 5′-monophosphate; AMP: adenosine monophosphate; ITP: inosine triphosphate; NAD: nicotinamide adenine dinucleotide. I: deionised water treatment; II: ultrasound treatment; III: acidic electrolysed water (AEW) treatment; IV: combination of AEW and ultrasound treatment.

[1] A positive value indicates an increase in the concentration of metabolites, and a negative value indicates a decrease in the concentration of metabolites.

[2] Within each row, means with different letters are significantly different among different treatments ($P < .05$).

aerobic conditions (Fernie, Carrari, & Sweetlove, 2004). In this study, the TCA cycle flux was repressed in planktonic *E. coli* after ultrasound and AEW combined treatment, according to the lower contents of TCA cycle related metabolites (Fig. 6A). Whereas in the air-dried *E. coli* cells, more active TCA activity was observed after combined stress, with higher contents of succinate and NAD, showing attached cells' resistance to adverse conditions (Fig. 6B). In fact, due to the decreased solubility of oxygen in AEW, lactate, acetate and ethanol in air-dried *E. coli* were produced through mixed acid fermentation, which could be served as shunts for maintaining glycolysis concomitantly (Ebrahimi et al., 2016). Besides, the pentose phosphate pathway (PPP) is also a shunt which can be served as an alternative to glycolysis, playing an important role in subsequent nucleotide synthesis and causing different level changes of nucleotides as mentioned in Section 3.4.

In addition to the degradation of glucose, TCA cycle is a key metabolic pathway connecting carbohydrate, fat and protein metabolism, due to many precursors and intermediates it can provide (Sweetlove, Beard, Nunes-Nesi, Fernie, & Ratcliffe, 2010). For example, alanine and aspartate are synthesised by the transamination of pyruvate and oxaloacetate, respectively, and the acetyl-CoA and citrate are associated with fatty acid degradation and synthesis, respectively. Therefore, as shown in Fig. 6, the disturbance of one metabolic trajectory could make whole *E. coli* metabolic network affected by ultrasound and AEW combined treatment, which was observed in both cultures.

Considering the pH of AEW in this study was around 3.8, *E. coli* might initiate a series of mechanisms to cope with acid stress, from

Table 3
Coefficients from OPLS-DA and metabolite contents in air-dried *E. coli* after different treatments.

Metabolites	Coefficient[1]					Contents (mg/L)[2]			
	II/I	III/I	IV/I	IV/II	IV/III	I	II	III	IV
Isoleucine	−0.98	−0.94	0.98	0.99	0.99	15.69 ± 0.27^{b}	13.80 ± 0.21^{c}	13.46 ± 0.07^{c}	18.37 ± 0.02^{a}
Leucine	−0.75	−0.60	0.94	0.98	0.99	1.73 ± 0.04^{b}	1.64 ± 0.02^{c}	1.70 ± 0.02^{bc}	1.97 ± 0.01^{a}
Valine	−0.80	−0.62	0.78	0.99	0.98	3.96 ± 0.11^{b}	3.51 ± 0.04^{d}	3.77 ± 0.03^{c}	4.29 ± 0.01^{a}
Ethanol	0.97	0.62	0.99	0.99	0.99	1.77 ± 0.04^{c}	3.97 ± 0.04^{b}	1.82 ± 0.04^{c}	10.95 ± 0.04^{a}
Lactate	−0.65	0.71	0.76	0.91	0.71	4.59 ± 0.21^{bc}	4.39 ± 0.03^{c}	4.71 ± 0.06^{b}	5.08 ± 0.03^{a}
Lysine	−0.70	0.99	0.99	0.99	0.99	42.82 ± 0.76^{c}	41.45 ± 0.57^{d}	60.69 ± 0.11^{b}	66.79 ± 0.23^{a}
Arginine	−0.62	−0.98	−0.82	0.73	0.97	7.48 ± 0.34^{a}	6.95 ± 0.15^{b}	4.36 ± 0.18^{c}	7.35 ± 0.15^{ab}
Acetate	−0.96	0.96	0.97	0.99	−0.82	4.64 ± 0.11^{c}	3.29 ± 0.05^{d}	8.28 ± 0.09^{a}	7.06 ± 0.01^{b}
Acetamide	−0.80	−0.84	0.90	0.98	0.77	1.95 ± 0.05^{b}	1.79 ± 0.02^{c}	1.80 ± 0.01^{c}	2.12 ± 0.01^{a}
β-aminoadipate	−0.97	0.42	−0.36	0.99	−0.57	70.90 ± 1.04^{a}	45.43 ± 0.85^{c}	72.23 ± 0.19^{a}	68.84 ± 0.26^{b}
Succinate	0.96	0.92	0.98	0.65	0.92	18.77 ± 0.25^{d}	34.14 ± 0.74^{b}	29.64 ± 0.11^{c}	39.80 ± 0.22^{a}
Aspartate	−0.96	−0.94	−0.99	−0.99	−0.96	60.03 ± 0.79^{a}	52.69 ± 0.38^{b}	51.47 ± 0.16^{b}	36.69 ± 0.64^{c}
Methylamine	0.75	−0.72	−0.78	−0.67	0.49	0.27 ± 0.01^{b}	0.30 ± 0.01^{a}	0.25 ± 0.01^{c}	0.26 ± 0.00^{bc}
γ-aminobutyrate	−0.95	0.92	0.92	0.99	0.98	69.19 ± 1.37^{c}	61.67 ± 0.71^{d}	89.91 ± 0.23^{b}	101.53 ± 0.28^{a}
Putrescine	0.97	−0.99	−0.99	−0.99	0.94	26.60 ± 0.23^{b}	30.18 ± 0.45^{a}	7.56 ± 0.05^{c}	8.07 ± 0.08^{c}
Betaine	−0.65	−0.82	−0.85	−0.73	0.86	3.17 ± 0.06^{a}	3.08 ± 0.03^{a}	2.57 ± 0.01^{a}	2.07 ± 1.22^{a}
Methanol	0.75	0.70	0.98	0.99	0.99	0.46 ± 0.02^{b}	0.52 ± 0.00^{b}	0.53 ± 0.01^{b}	7.37 ± 0.12^{a}
Taurine	−0.98	0.74	−0.97	−0.97	−0.99	25.58 ± 0.70^{b}	19.92 ± 0.10^{c}	29.29 ± 0.23^{a}	17.05 ± 0.08^{d}
Glycine	−0.99	−0.98	−0.99	−0.99	−0.99	7.80 ± 0.12^{a}	5.79 ± 0.07^{c}	7.00 ± 0.02^{b}	3.49 ± 0.01^{d}
Alanine	−0.98	0.87	−0.99	0.91	−0.99	187.44 ± 2.02^{b}	137.19 ± 2.24^{d}	195.93 ± 0.36^{a}	154.52 ± 0.55^{c}
Glutamate	−0.98	0.65	−0.99	0.91	−0.99	271.34 ± 4.10^{a}	190.85 ± 2.29^{c}	274.90 ± 0.56^{a}	223.75 ± 1.17^{b}
Uridine	−0.99	−0.86	0.81	0.99	0.99	92.97 ± 0.86^{b}	76.61 ± 2.00^{d}	87.95 ± 0.22^{c}	98.52 ± 0.62^{a}
Glyceric acid	−0.98	0.73	−0.98	0.98	−0.99	45.18 ± 0.45^{a}	32.07 ± 0.43^{c}	44.78 ± 0.06^{a}	39.95 ± 0.26^{b}
Phosphorylcholine	−0.99	0.99	0.99	0.84	−0.98	/	/	/	/
N-acetyl alanine	−0.93	0.99	0.97	0.93	−0.99	/	/	/	/
β-glucose	−0.97	0.64	−0.71	0.94	−0.91	36.89 ± 0.72^{b}	23.85 ± 0.23^{d}	38.20 ± 0.44^{a}	34.62 ± 0.60^{c}
Phosphoenolpyruvate	−0.98	0.60	−0.87	0.96	−0.91	38.38 ± 0.23^{a}	24.07 ± 0.62^{c}	38.99 ± 0.16^{a}	36.44 ± 0.17^{b}
α-glucose	−0.95	0.81	0.87	0.93	−0.77	2.09 ± 0.08^{c}	1.44 ± 0.07^{d}	2.80 ± 0.09^{a}	2.44 ± 0.04^{b}
Ribose-5-phosphate	0.65	0.84	−0.61	−0.88	−0.96	6.81 ± 0.32^{c}	7.37 ± 0.18^{b}	8.26 ± 0.18^{a}	6.19 ± 0.04^{d}
Cytidine	−0.85	−0.52	0.66	0.80	0.68	22.20 ± 0.09^{b}	19.39 ± 0.58^{d}	21.09 ± 0.21^{c}	23.97 ± 0.06^{a}
Adenosine 2′-3′-cyclic phosphate	−0.98	−0.83	−0.92	0.93	0.98	18.23 ± 0.29^{a}	10.55 ± 0.73^{d}	12.01 ± 0.24^{c}	15.00 ± 0.13^{b}
Fumarate	0.78	−0.97	−0.98	−0.97	0.45	2.17 ± 0.10^{b}	2.83 ± 0.14^{a}	0.38 ± 0.02^{c}	0.46 ± 0.01^{c}
Tyrosine	−0.45	−0.80	−0.88	−0.73	−0.50	1.93 ± 0.04^{a}	1.72 ± 0.09^{b}	1.40 ± 0.09^{c}	1.27 ± 0.05^{c}
Xanthine	−0.91	0.95	0.75	0.98	−0.66	2.36 ± 0.04^{c}	1.44 ± 0.07^{d}	3.32 ± 0.06^{a}	3.16 ± 0.06^{b}
UMP	−0.99	−0.79	0.83	0.99	0.89	7.53 ± 0.02^{b}	4.10 ± 0.11^{c}	7.51 ± 0.06^{b}	8.09 ± 0.02^{a}
Hypoxanthine	−0.56	−0.81	0.83	0.81	0.74	7.36 ± 0.12^{ab}	7.05 ± 0.23^{bc}	6.77 ± 0.13^{c}	7.55 ± 0.04^{a}
AMP	−0.77	−0.96	−0.95	0.75	0.66	14.42 ± 0.42^{a}	8.51 ± 0.73^{b}	7.32 ± 0.29^{c}	9.30 ± 0.08^{b}
Formate	−0.74	−0.90	0.72	0.79	0.94	3.87 ± 0.04^{b}	3.55 ± 0.07^{d}	3.71 ± 0.02^{c}	4.40 ± 0.02^{a}
ITP	−0.75	0.98	0.94	0.91	0.96	6.16 ± 0.10^{c}	5.03 ± 0.43^{d}	8.04 ± 0.18^{b}	9.92 ± 0.14^{a}
NAD	−0.58	−0.51	0.67	0.74	0.75	54.23 ± 0.75^{b}	52.05 ± 1.34^{c}	53.14 ± 0.19^{bc}	61.24 ± 0.31^{a}

Note: UMP: uridine 5′-monophosphate; AMP: adenosine monophosphate; ITP: inosine triphosphate; NAD: nicotinamide adenine dinucleotide. I: deionised water treatment; II: ultrasound treatment; III: acidic electrolysed water (AEW) treatment; IV: combination of AEW and ultrasound treatment. /The concentration was not determined due to signal overlapping.

[1] A positive value indicates an increase in the concentration of metabolites, and a negative value indicates a decrease in the concentration of metabolites.

[2] Within each row, means with different letters are significantly different among different treatments ($P < .05$).

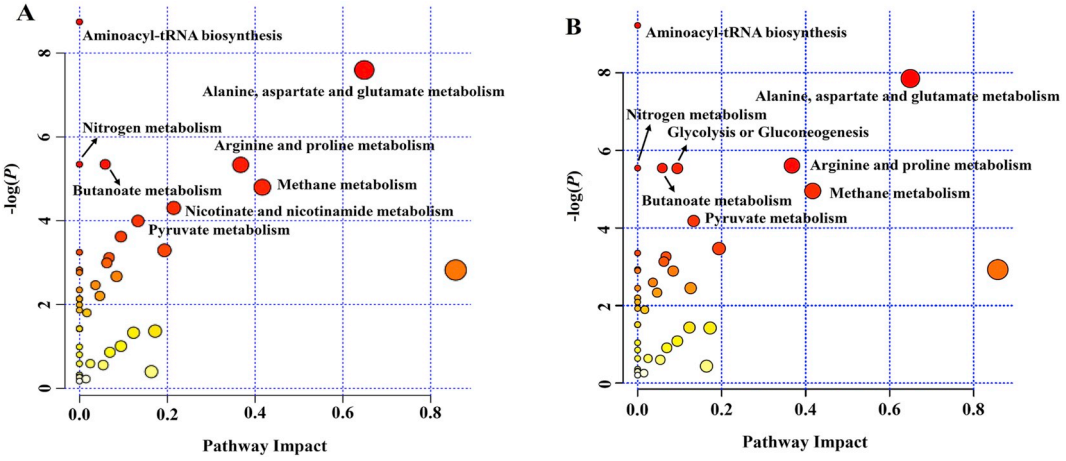

Fig. 5. Overview of the pathway analysis of planktonic *E. coli* (A) and air-dried *E. coli* (B). Each circle represents one pathway, and the colour and size of each circle is based on the *P* value and the pathway impact value, respectively.

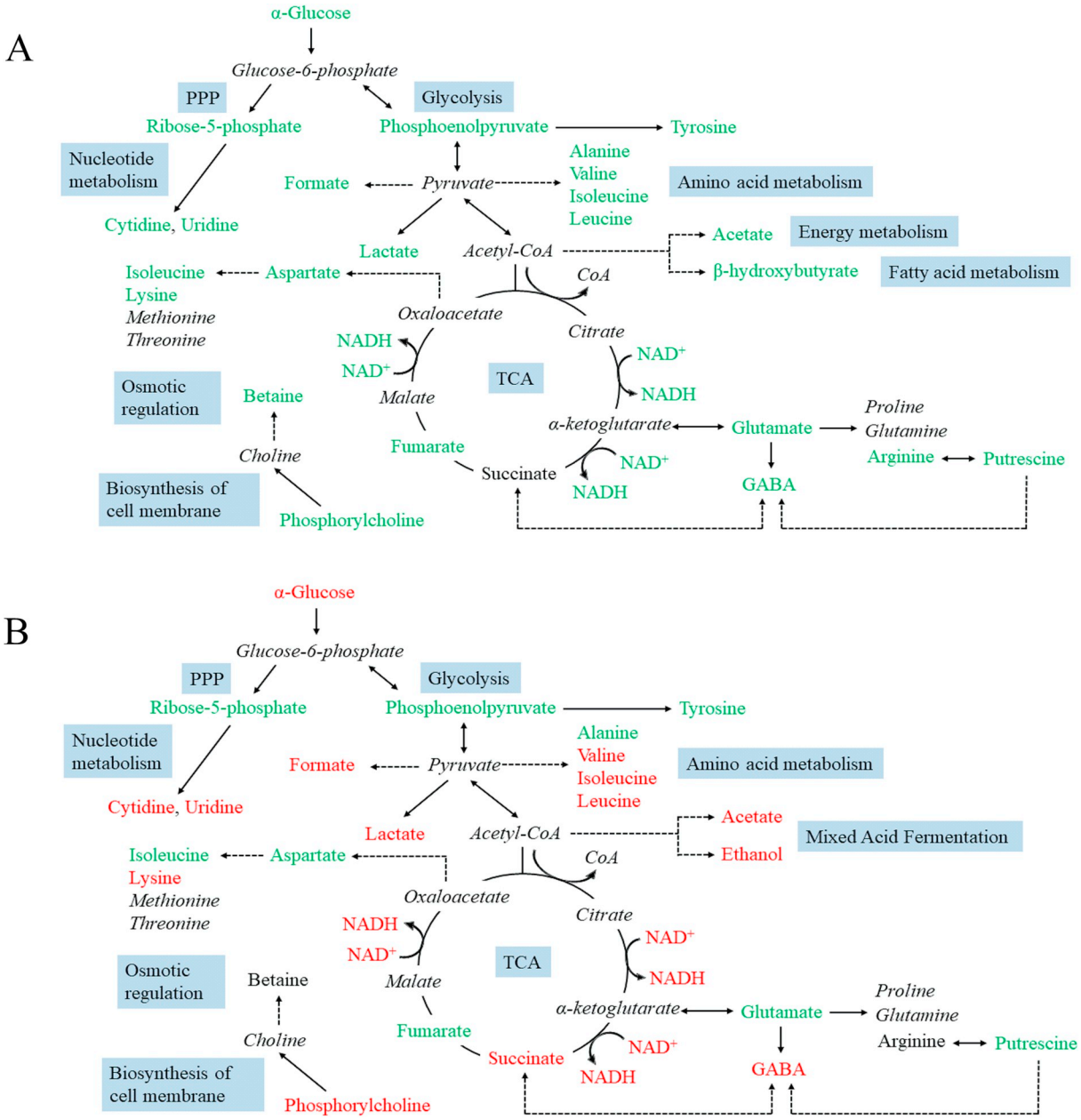

Fig. 6. Proposed schematic of metabolic alterations upon ultrasound and AEW combined treatment in planktonic *E. coli* (A) and air-dried *E. coli* (B). Metabolites coloured in green, red or black represent lower, higher or similar level in ultrasound + AEW treated *E. coli* compared to the control group, respectively. Metabolites in italic black were not detected. (For interpretation of the references to colour in this figure legend, the reader is referred to the web version of this article.)

transcriptional and translational aspects. Lund, Tramonti, and De Biase (2014) summarised several mechanisms *E. coli* adopts to survive in acid environment, including deiminase and deaminase systems, F_1-F_0 ATPase, amino acid-dependent decarboxylase/antiporter systems and modifications of cell membrane. In this study, putrescine, a polyamine related to cell division, was detected in both states of *E. coli*. It was reported that *potABD* (encoding spermidine/putrescine import protein) and *speB* (encoding an enzyme catalysing the formation of putrescine) could be upregulated in *E. coli* with a high growth rate (Gutierrez-Ríos et al., 2007). Therefore, a decrease in putrescine levels in both two cultured *E. coli* revealed an inhibited growth due to the ultrasound and AEW stresses in our work. Additionally, its precursor, glutamate, offers acid-stress protection to *E. coli* through glutamate decarboxylase system, with the help of two glutamate decarboxylase isozymes (GadA and GadB), either of which can bind cytoplasmic protons to produce γ-aminobutyrate (GABA). After then, GABA is exported from the bacterial cytoplasm to exchange with extracellular glutamate by GadC antiporter (Bearson, Lee, & Casey, 2009). The higher contents of GABA and succinate and lower contents of glutamate and putrescine were observed in air-dried *E. coli* after ultrasound and AEW combined treatment, indicating putrescine served as a good source to be converted into GABA and succinate to maintain TCA cycle and enhance acid resistance. Whereas in the planktonic culture, the decreased levels of above metabolites showed its sensitivity and poor resistance to the combined sanitising treatments.

In addition to acid stress, oxidative and osmotic stresses (mentioned in Section 3.4) also caused intracellular damage in our work. Thus, other systems like OxyR- and RpoS-dependent stress response systems might also be involved against the damage, with their genes upregulated in AEW exposed cells as suggested in former studies (Liu, 2018). Besides, choline is a chemical chaperone that plays a role in the maintenance of structural integrity and synthesis of cell membranes, as

well as can be metabolised into betaine, offering osmoprotective effect (Michel, Yuan, Ramsubir, & Bakovic, 2006). In this study, the higher level of phosphorylcholine (choline precursor) and stable level of betaine were identified in air-dried *E. coli*, a fact not observed in planktonic cells, indicating attached cells' attempt to repair the damage under ultrasound and AEW stresses, which might be beyond the range of planktonic cells' ability.

4. Conclusion

The analysis of global metabolomic responses of planktonic and air-dried *E. coli* to ultrasound and AEW stresses were investigated in this study. The two states of *E. coli* responded quite differently to the combined treatment, with different concentration changes in amino acids, organic acids and nucleotides. Further analysis revealed that these metabolite changes were associated with disturbed energy metabolism, altered amino acid metabolism and depressed growth pattern, which were identified in both two states of *E. coli* but to different extent, as air-dried *E. coli* exhibited more resistance to adverse conditions. This study shows that NMR-based metabolomics strategy was effective to identify the stress effects that ultrasound and AEW caused and to elucidate global metabolic differences between different states of bacteria, providing an example for future mechanism studies as well as some guidance for food contact surface sanitisation.

Declaration of Competing Interest

We declare that we do not have any commercial or associative interest that represents a conflict of interest in connection with this manuscript. We have no financial and personal relationships with other people or organizations that can inappropriately influence our work.

Acknowledgements

This study was funded by the Singapore Ministry of Education Academic Research Fund Tier 1 (R-143-000-A40-114), project 31371851 supported by NSFC, Natural Science Foundation of Jiangsu Province (BK20181184) and an industry grant supported by Shenzhen Zhiyun Optoelectronics Co., Ltd. (R-143-000-A24-597).

Appendix A. Supplementary data

Supplementary data to this article can be found online at https://doi.org/10.1016/j.foodres.2019.108607.

References

Adhikari, A., Syamaladevi, R. M., Killinger, K., & Sablani, S. S. (2015). Ultraviolet-C light inactivation of *Escherichia coli* O157:H7 and *Listeria monocytogenes* on organic fruit surfaces. *International Journal of Food Microbiology, 210*, 136–142.

Bastarrachea, L. J., Walsh, M., Wrenn, S. P., & Tikekar, R. V. (2017). Enhanced antimicrobial effect of ultrasound by the food colorant Erythrosin B. *Food Research International, 100*, 344–351.

Bearson, B. L., Lee, I. S., & Casey, T. A. (2009). *Escherichia coli* O157:H7 glutamate-and arginine-dependent acid-resistance systems protect against oxidative stress during extreme acid challenge. *Microbiology, 155*(3), 805–812.

Bisht, H., Bhatnagar, M., Bisht, S., & Murthy, A. K. (2018). Study on variation of polar metabolites in control and water stressed *Gossypium hirsutum* L. using NMR spectroscopy. *Asian Journal of Applied Chemistry Research, 1*(3), 1–12.

Booth, S. C., Workentine, M. L., Wen, J., Shaykhutdinov, R., Vogel, H. J., Ceri, H., ... Weljie, A. M. (2011). Differences in metabolism between the biofilm and planktonic response to metal stress. *Journal of Proteome Research, 10*(7), 3190–3199.

Chen, L., Wu, J. E., Li, Z., Liu, Q., Zhao, X., & Yang, H. (2019). Metabolomic analysis of energy regulated germination and sprouting of organic mung bean (*Vigna radiata*) using NMR spectroscopy. *Food Chemistry, 286*, 87–97.

Chen, L., Zhang, H., Liu, Q., Pang, X., Zhao, X., & Yang, H. (2019). Sanitising efficacy of lactic acid combined with low-concentration sodium hypochlorite on *Listeria innocua* in organic broccoli sprouts. *International Journal of Food Microbiology, 295*, 41–48.

Ebrahimi, P., Larsen, F. H., Jensen, H. M., Vogensen, F. K., & Engelsen, S. B. (2016). Real-time metabolomic analysis of lactic acid bacteria as monitored by in vitro NMR and chemometrics. *Metabolomics, 12*(4), 77.

Feng, H., Yang, W., & Hielscher, T. (2008). Power ultrasound. *Food Science and Technology International, 14*(5), 433–436.

Fernie, A. R., Carrari, F., & Sweetlove, L. J. (2004). Respiratory metabolism: Glycolysis, the TCA cycle and mitochondrial electron transport. *Current Opinion in Plant Biology, 7*(3), 254–261.

Gjersing, E. L., Herberg, J. L., Horn, J., Schaldach, C. M., & Maxwell, R. S. (2007). NMR metabolomics of planktonic and biofilm modes of growth in *Pseudomonas aeruginosa*. *Analytical Chemistry, 79*(21), 8037–8045.

Gutierrez-Ríos, R. M., Freyre-Gonzalez, J. A., Resendis, O., Collado-Vides, J., Saier, M., & Gosset, G. (2007). Identification of regulatory network topological units coordinating the genome-wide transcriptional response to glucose in *Escherichia coli*. *BMC Microbiology, 7*(1), 53.

Harvey, R. R., Zakhour, C. M., & Gould, L. H. (2016). Foodborne disease outbreaks associated with organic foods in the United States. *Journal of Food Protection, 79*(11), 1953–1958.

Heaton, J. C., & Jones, K. (2008). Microbial contamination of fruit and vegetables and the behaviour of enteropathogens in the phyllosphere: A review. *Journal of Applied Microbiology, 104*(3), 613–626.

Hussain, M. S., Tango, C. N., & Oh, D. H. (2019). Inactivation kinetics of slightly acidic electrolyzed water combined with benzalkonium chloride and mild heat treatment on vegetative cells, spores, and biofilms of *Bacillus cereus*. *Food Research International, 116*, 157–167.

Jozefczuk, S., Klie, S., Catchpole, G., Szymanski, J., Cuadros-Inostroza, A., Steinhauser, D., ... Willmitzer, L. (2010). Metabolomic and transcriptomic stress response of *Escherichia coli*. *Molecular Systems Biology, 6*(1), 364.

Kim, H., Ryu, J.-H., & Beuchat, L. R. (2007). Effectiveness of disinfectants in killing *Enterobacter sakazakii* in suspension, dried on the surface of stainless steel, and in a biofilm. *Applied and Environmental Microbiology, 73*(4), 1256–1265.

Li, J., Ding, T., Liao, X., Chen, S., Ye, X., & Liu, D. (2017). Synergetic effects of ultrasound and slightly acidic electrolyzed water against *Staphylococcus aureus* evaluated by flow cytometry and electron microscopy. *Ultrasonics Sonochemistry, 38*, 711–719.

Li, J., Ma, L., Liao, X., Liu, D., Lu, X., Chen, S., ... Ding, T. (2018). Ultrasound-induced *Escherichia coli* O157:H7 cell death exhibits physical disruption and biochemical apoptosis. *Frontiers in Microbiology, 9*, 2486.

Liu, Q. (2018). *Effects of electrolysed water combined with mild heat on bacterial metabolic response and quality of fresh organic produce.* National University of Singapore: Dissertation/Thesis.

Liu, Q., Jin, X., Feng, X., Yang, H., & Fu, C. (2019). Inactivation kinetics of *Escherichia coli* O157:H7 and *Salmonella* Typhimurium on organic carrot (*Daucus carota* L.) treated with low concentration electrolyzed water combined with short-time heat treatment. *Food Control, 106*, 106702.

Liu, Q., Wu, J. E., Lim, Z. Y., Aggarwal, A., Yang, H., & Wang, S. (2017). Evaluation of the metabolic response of *Escherichia coli* to electrolysed water by ^{1}H NMR spectroscopy. *LWT – Food Science and Technology, 79*, 428–436.

Liu, Q., Wu, J. E., Lim, Z. Y., Lai, S., Lee, N., & Yang, H. (2018). Metabolite profiling of *Listeria innocua* for unravelling the inactivation mechanism of electrolysed water by nuclear magnetic resonance spectroscopy. *International Journal of Food Microbiology, 271*, 24–32.

Lou, X., Ye, Y., Wang, Y., Sun, Y., Pan, D., & Cao, J. (2018). Effect of high-pressure treatment on taste and metabolite profiles of ducks with two different vinasse-curing processes. *Food Research International, 105*, 703–712.

Lund, P., Tramonti, A., & De Biase, D. (2014). Coping with low pH: Molecular strategies in neutralophilic bacteria. *FEMS Microbiology Reviews, 38*(6), 1091–1125.

Lushchak, V. I. (2011). Adaptive response to oxidative stress: Bacteria, fungi, plants and animals. *Comparative Biochemistry and Physiology Part C: Toxicology & Pharmacology, 153*(2), 175–190.

Maifreni, M., Frigo, F., Bartolomeoli, I., Buiatti, S., Picon, S., & Marino, M. (2015). Bacterial biofilm as a possible source of contamination in the microbrewery environment. *Food Control, 50*, 809–814.

Malmendal, A., Overgaard, J., Bundy, J. G., Sørensen, J. G., Nielsen, N. C., Loeschcke, V., & Holmstrup, M. (2006). Metabolomic profiling of heat stress: Hardening and recovery of homeostasis in *Drosophila*. *American Journal of Physiology—Regulatory, Integrative and Comparative Physiology, 291*(1), R205–R212.

Michel, V., Yuan, Z., Ramsubir, S., & Bakovic, M. (2006). Choline transport for phospholipid synthesis. *Experimental Biology and Medicine, 231*(5), 490–504.

Miranda, R. O., Campos-Galvão, M. E. M., & Nero, L. A. (2018). Expression of genes associated with stress conditions by *Listeria monocytogenes* in interaction with nisin producer *Lactococcus lactis*. *Food Research International, 105*, 897–904.

National Organic Program (2011). The use of chlorine materials in organic production & handling. NOP 5026 https://www.ams.usda.gov/sites/default/files/media/5026.pdf, Accessed date: 10 June 2019.

Nicholson, J. K., & Lindon, J. C. (2008). Systems biology: Metabonomics. *Nature, 455*(7216), 1054.

Nightingale, Z. D., Lancha, A. H., Jr., Handelman, S. K., Dolnikowski, G. G., Busse, S. C., Dratz, E. A., ... Handelman, G. J. (2000). Relative reactivity of lysine and other peptide-bound amino acids to oxidation by hypochlorite. *Free Radical Biology and Medicine, 29*(5), 425–433.

Odeyemi, O. A., Burke, C. M., Bolch, C. J., & Stanley, R. (2018). Evaluation of spoilage potential and volatile metabolites production by *Shewanella baltica* isolated from modified atmosphere packaged live mussels. *Food Research International, 103*, 415–425.

Sagong, H. G., Cheon, H. L., Kim, S. O., Lee, S. Y., Park, K. H., Chung, M. S., ... Kang, D. H. (2013). Combined effects of ultrasound and surfactants to reduce *Bacillus cereus* spores on lettuce and carrots. *International Journal of Food Microbiology, 160*(3), 367–372.

Salaheen, S., Jaiswal, E., Joo, J., Peng, M., Ho, R., OConnor, D., ... Biswas, D. (2016).

Bioactive extracts from berry byproducts on the pathogenicity of *Salmonella* Typhimurium. *International Journal of Food Microbiology, 237*, 128–135.
Sánchez, G., Elizaquível, P., Aznar, R., & Selma, M. (2015). Virucidal effect of high power ultrasound combined with a chemical sanitizer containing peroxyacetic acid for water reconditioning in the fresh-cut industry. *Food Control, 52*, 126–131.
Sow, L. C., Tirtawinata, F., Yang, H., Shao, Q., & Wang, S. (2017). Carvacrol nanoemulsion combined with acid electrolysed water to inactivate bacteria, yeast *in vitro* and native microflora on shredded cabbages. *Food Control, 76*, 88–95.
Sweetlove, L. J., Beard, K. F., Nunes-Nesi, A., Fernie, A. R., & Ratcliffe, R. G. (2010). Not just a circle: Flux modes in the plant TCA cycle. *Trends in Plant Science, 15*(8), 462–470.
USDA (2019). organic regulations 7 CFR 205.605. https://www.ecfr.gov/cgi-bin/text-idx?SID=914ec2697257324452b3c52e2b00246b&mc=true&node=se7.3.205_1605&rgn=div8, Accessed date: 24 July 2019.
Velmurugan, R., & Incharoensakdi, A. (2016). Proper ultrasound treatment increases ethanol production from simultaneous saccharification and fermentation of sugarcane bagasse. *RSC Advances, 6*(94), 91409–91419.
Villas-Bôas, S. G., Mas, S., Åkesson, M., Smedsgaard, J., & Nielsen, J. (2005). Mass spectrometry in metabolome analysis. *Mass Spectrometry Reviews, 24*(5), 613–646.
Wall, S. B., Oh, J.-Y., Diers, A. R., & Landar, A. (2012). Oxidative modification of proteins: An emerging mechanism of cell signaling. *Frontiers in Physiology, 3*, 369.
Wiklund, S., Johansson, E., Sjöström, L., Mellerowicz, E. J., Edlund, U., Shockcor, J. P., ... Trygg, J. (2008). Visualization of GC/TOF-MS-based metabolomics data for identification of biochemically interesting compounds using OPLS class models. *Analytical Chemistry, 80*(1), 115–122.
Ye, Y., Zhang, L., Hao, F., Zhang, J., Wang, Y., & Tang, H. (2012). Global metabolomic responses of *Escherichia coli* to heat stress. *Journal of Proteome Research, 11*(4), 2559–2566.
Ye, Y., Zhang, L., Yang, R., Luo, Q., Chen, H., Yan, X., & Tang, H. (2013). Metabolic phenotypes associated with high-temperature tolerance of *Porphyra haitanensis* strains. *Journal of Agricultural and Food Chemistry, 61*(35), 8356–8363.
Yu, X., & Yang, H. (2017). Pyrethroid residue determination in organic and conventional vegetables using liquid-solid extraction coupled with magnetic solid phase extraction based on polystyrene-coated magnetic nanoparticles. *Food Chemistry, 217*, 303–310.
Zhang, J., & Yang, H. (2017). Effects of potential organic compatible sanitisers on organic and conventional fresh-cut lettuce (*Lactuca sativa* Var. *Crispa* L). *Food Control, 72*, 20–26.
Zhao, L., Zhang, Y., & Yang, H. (2017). Efficacy of low concentration neutralised electrolysed water and ultrasound combination for inactivating *Escherichia coli* ATCC 25922, *Pichia pastoris* GS115 and *Aureobasidium pullulans* 2012 on stainless steel coupons. *Food Control, 73*, 889–899.
Zhao, L., Zhao, M. Y., Phey, C. P., & Yang, H. (2019). Efficacy of low concentration acidic electrolysed water and levulinic acid combination on fresh organic lettuce (*Lactuca sativa* Var. *Crispa* L.) and its antimicrobial mechanism. *Food Control, 101*, 241–250.
Zhao, X., Wu, J. E., Chen, L., & Yang, H. (2019). Effect of vacuum impregnated fish gelatin and grape seed extract on metabolite profiles of tilapia (*Oreochromis niloticus*) fillets during storage. *Food Chemistry, 293*, 418–428.